Core-Annular Two-Phase Flow in a Gently Curved Circular Channel

J. R. Picardo and S. Pushpavanam
Dept. of Chemical Engineering, Indian Institute of Technology Madras, Chennai, 600 036 India

DOI 10.1002/aic.14247
Published online October 30, 2013 in Wiley Online Library (wileyonlinelibrary.com)

The velocity field of a core-annular two-phase flow through a curved channel is investigated. The case of fully developed flow with a concentric, circular fluid–fluid interface is considered. In the limit of a gentle axial curvature of the curved channel, an analytical solution is obtained in the form of a regular asymptotic expansion to first order. The condition on the physical parameters for the core to be concentric and circular is derived by accounting for the normal stresses at the interface. Two key features of the flow, the secondary circulations and the redistribution of the axial velocity, are described in detail. The viscous coupling of the two fluids at the interface leads to a variety of circulation patterns and axial velocity profiles, depending on the system parameters. The parameter space is divided into different regions using analytical conditions at the transition between flow regimes. © 2013 American Institute of Chemical Engineers *AIChE J*, 59: 4871–4886, 2013
Keywords: core-annular, curved channel, asymptotic solution, secondary vortices

Introduction

Core-annular (CA) flow refers to a two-phase flow configuration in which one fluid occupies the central core of a circular channel while the other fills the annular region. Such flows have received much attention in the context of water lubricated transport of oil.[1] Recently, core-annular flow in microchannels has become a subject of considerable theoretical and practical interest. *Stable* core-annular flow in microchannels has been studied *experimentally* by several workers.[2–6]

As fluid flows through a curved channel it experiences a transverse centrifugal force. The magnitude of this force is determined by the local axial velocity of the fluid. A viscous fluid has a radially varying axial velocity profile. The velocity is greater at the center of the channel and falls off to zero at the channel walls. Hence, there is a spatial variation of the centrifugal force across the cross section of the curved channel. This induces several hydrodynamic features which distinguish curved channel flows from their straight channel counterparts. Apart from being theoretically intriguing, curvature induced effects, such as secondary circulations and particle migration, form the basis of several applications. These include applications at the macroscale in process industries as well as in emerging microfluidic technologies.[7,8] This is true of both single- and two-phase flows.

Single-phase flows in curved channels have received extensive attention and are relatively well-understood. The first theoretical analysis was presented by Dean.[9,10] He obtained an approximate analytical result in the asymptotic limit of a gently curved channel; a channel for which the radius of the cross section is small in comparison with the radius of curvature of the channel. The system exhibits a secondary flow pattern of two counter-rotating vortices (Dean vortices). The axial velocity profile is not axisymmetric. Moreover, the flow rate is lower in the curved channel as compared to a straight channel for a given average axial pressure gradient. Extensive work has been done since then on the single-phase problem, accounting for finite curvature, high Reynolds numbers, developing flow and noncircular cross sections. The significant results are discussed in the reviews by Berger et al.[11] and Vashisth et al.[7]

In contrast, very few fundamental studies exist on two-phase flow in curved channels and little information is available on circulation patterns and velocity profiles.[7] Only recently have these problems been receiving due attention. Slug and bubble flow has been analyzed by Muradoglu & Stone[12] and Kumar et al.[13] while Ghosh et al. present simulations of core-annular flow in curved bends.[14] On the other hand, there is a considerable body of experimental results available on pressure drop, volume fractions and flow regime maps.[3,15–18] Recent experimental results demonstrate the strong influence of curved sections on two-phase flow patterns.[17,19] Some of these flow patterns are unique to the curved geometry, e.g., annular-dispersed flow as reported by Sarkar et al.[3] Hence, there is considerable motivation to analyze two-phase, curved channel flows in detail.

The key feature of the core-annular (CA) flow which distinguishes it from its single-phase counterpart is the interaction between the two fluids at the fluid–fluid interface. One must consider the continuity of velocity at the interface and account for the mutual exertion of stresses by the fluids. This viscous coupling of the flow in the core fluid with that in the annular fluid is responsible for several novel features

Additional Supporting Information may be found in the online version of this article.

Correspondence concerning this article should be addressed Pushpavanam at spush@iitm.ac.in.

of the velocity field. Hypothetically, if the fluids were to be decoupled, the natural circulatory flow in each fluid would be in opposite directions at the interface. The resolution of this contradiction results in a rich variety of possible flow patterns. In fact, it is possible for one of the fluids to dominate and dictate the flow of the other.

Apart from inducing secondary circulations within each fluid, the centrifugal force may be expected to cause a displacement of the core fluid away from the center of the channel. This feature has been observed experimentally in small channels with curved bends by Sarkar et al.[3] and Ghosh et al.[14] However, this is *not* always the case. Depending on the physical parameters (e.g., density ratio) the core fluid may be displaced toward the inner or outer side of the channel. Hence, a set of parameters must exist for which the core remains circular and concentric with the channel. A formal justification for a concentric core solution is presented in this work. The subset of parameters for which this flow will be realized is determined by imposing the normal stress balance at the circular interface. In this work, we focus on this case of a fully developed flow with a concentric, circular core. Within this setting, the interfluid interaction via the mutual exertion of viscous shear stress at the interface can be studied most clearly. Moreover, it is amenable to an analytical result which facilitates a detailed understanding of the prominent physical mechanisms governing the flow. The results and conclusions of this study of concentric CA flow will aid in future investigations of the more general problem in which the core is nonconcentric and noncircular.

In keeping with the spirit of the early single-phase investigations,[9,20] we consider the asymptotic limit of a gently curved circular channel. This is the case where in ε, the ratio of the radius of the circular cross section to the radius of curvature of the channel, is small ($\varepsilon \ll 1$). An approximate analytical solution is derived using a regular asymptotic expansion to $O(\varepsilon^1)$. The effect of varying the fluid properties and operating conditions is studied in detail and we find a rich variety of flow features and circulation patterns.

It is important to note that the flow described here may be observed in a laboratory only if the mathematical solution (steady state) is stable. The stability of core-annular flow in *straight* channels has been studied extensively. The key results of linear stability analyses, summarized by Joseph et al.[1] indicates that core-annular flows can be *stable* if the core fluid is more viscous and the Reynolds numbers are moderately high. At low Reynolds number, the jet is susceptible to capillary breakup while at large Reynolds number the interface becomes unstable due to viscosity differences between the fluids. In general, CA flows with a relatively large core are more stable. In *microchannels*, stable CA flows have been reported in both straight channels and curved bends.[3] Stable flows have been observed with a more viscous core[2,3] as well as a less viscous core, provided the core is large and strongly confined by the walls of the microchannel.[3,4] On the other hand, thin cores are stable only if the core fluid is significantly more viscous than the annular fluid.[2] As expected from stability theory, the flows are stable only at relatively high-flow rates. The dominance of viscous forces in microchannels leads to low-growth rates of the capillary instability and promotes stable CA flow. Recent experiments on novel aqueous two-phase systems (ATPS) have shown that CA flow can persist in these systems over very long length scales- an order of magnitude longer than conventional oil–water two-phase systems with comparable surface tension.[5] This is attributed to the special features of the interface in ATPS which are as yet not clearly understood.[5] CA flows with ATPS have been applied to separate biomolecules efficiently.[6] The stability theory of CA flow in a *curved channel* is not yet developed. A possible first step would be to carry out a linear stability analysis using the solution provided in this work as a base flow.

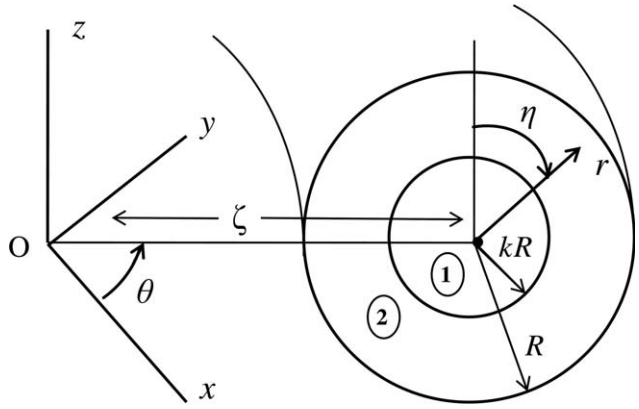

Figure 1. Schematic of the CA flow configuration showing the orthogonal curvilinear coordinate system (r,η,θ) and its relation with the Cartesian system (x,y,z) (Not drawn to scale for the sake of clarity).

Coordinate System and Governing Equations

Consider a curved channel of circular cross section in which a fully developed core-annular flow with a circular, concentric interface has been established. R is the radius of the cross section, while ζ is the radius of curvature of the channel. The core has a radius kR. The orthogonal, curvilinear coordinate system used by Dean[9] is adopted here. A schematic of the coordinate system is presented in Figure 1. The mapping between this curvilinear coordinate system and the cartesian coordinate system is given by Eq.1. The z-axis coincides with the axis about which the channel curves

$$\left.\begin{aligned} x &= \zeta\cos\theta + r\sin\eta\cos\theta \\ y &= \zeta\sin\theta + r\sin\eta\sin\theta \\ z &= r\cos\eta \end{aligned}\right\} \tag{1}$$

The continuity and the Navier-Stokes equations in this curvilinear coordinate system, for an incompressible fluid in steady, fully developed flow are presented below. The subscript i is an index which denotes the fluids; $i = 1$ denotes the core fluid, and $i = 2$ the annular fluid. The variables have been scaled with the following characteristic scales, denoted by the subscript (c). The superscript (*) indicates dimensional flow variables

$$r_c = R;\ w_{i,c} = u_{i,c} = v_{i,c} = \frac{R^2}{\mu_i}\left(\frac{1}{\zeta}\frac{\partial P_i^*}{\partial\theta}\right) = \frac{GR^2}{\mu_i};\ P_{i,c} = \frac{w_{i,c}\mu_i}{R} = GR; \tag{2}$$

u, v, w are the velocity components along the r, η, θ coordinate directions, respectively. G is the constant pressure gradient imposed along the axial centerline of the channel (θ coordinate line through $r = 0$), i.e. $G = \frac{1}{\zeta}\frac{\partial P_i^*}{\partial\theta}$. Five dimensionless quantities arise as a result of this scaling. These are the

Reynolds numbers (Re_1 and Re_2), viscosity ratio (μ_1/μ_2), the fractional core radius (k), and the curvature ratio (ε)

$$\mathrm{Re}_i=\frac{\rho_i w_{i,c} R}{\mu_i}=\frac{\rho_i G R^3}{\mu_i^2};\quad \varepsilon=\frac{R}{\zeta} \tag{3}$$

The resulting mass and momentum balance equations in dimensionless form are

$$\frac{\partial u_i}{\partial r}+\frac{u_i}{r}+\frac{1}{r}\frac{\partial v_i}{\partial \eta}+\varepsilon\frac{(u_i\sin\eta+v_i\cos\eta)}{(1+r\varepsilon\sin\eta)}=0 \tag{4}$$

$$\mathrm{Re}_i\left[u_i\frac{\partial u_i}{\partial r}+\frac{v_i}{r}\frac{\partial u_i}{\partial \eta}-\frac{{v_i}^2}{r}-\varepsilon\frac{{w_i}^2\sin\eta}{(1+r\varepsilon\sin\eta)}\right]=-\frac{\partial P_i}{\partial r}-\left[\left(\frac{1}{r}\frac{\partial}{\partial\eta}+\varepsilon\frac{\cos\eta}{(1+r\varepsilon\sin\eta)}\right)\quad\left(\frac{\partial v_i}{\partial r}+\frac{v_i}{r}-\frac{1}{r}\frac{\partial u_i}{\partial\eta}\right)\right] \tag{5}$$

$$\mathrm{Re}_i\left[u_i\frac{\partial v_i}{\partial r}+\frac{v_i}{r}\frac{\partial v_i}{\partial \eta}+\frac{v_i u_i}{r}-\varepsilon\frac{{w_i}^2\cos\eta}{(1+r\varepsilon\sin\eta)}\right]=-\frac{1}{r}\frac{\partial P_i}{\partial\eta}+\left[\left(\frac{\partial}{\partial r}+\varepsilon\frac{\sin\eta}{(1+r\varepsilon\sin\eta)}\right)\quad\left(\frac{\partial v_i}{\partial r}+\frac{v_i}{r}-\frac{1}{r}\frac{\partial u_i}{\partial\eta}\right)\right] \tag{6}$$

$$\mathrm{Re}_i\left[u_i\frac{\partial w_i}{\partial r}+\frac{v_i}{r}\frac{\partial w_i}{\partial \eta}+\varepsilon\frac{(w_i u_i\sin\eta+w_i v_i\cos\eta)}{(1+r\varepsilon\sin\eta)}\right]=-\frac{1}{(1+r\varepsilon\sin\eta)}+\left[\left(\frac{\partial}{\partial r}+\frac{1}{r}\right)\left(\frac{\partial w_i}{\partial r}+\varepsilon\frac{w_i\sin\eta}{(1+r\varepsilon\sin\eta)}\right)+\frac{1}{r}\frac{\partial}{\partial\eta}\left(\frac{1}{r}\frac{\partial w_i}{\partial\eta}+\varepsilon\frac{w_i\cos\eta}{(1+r\varepsilon\sin\eta)}\right)\right] \tag{7}$$

These equations for the core ($i=1$) and annular ($i=2$) fluids are applicable in their respective domains, i.e. $0<r<k$ for $i=1$ and $k<r<1$ for $i=2$.

The aforementioned form of the equations is obtained by substituting $\nabla^2\overline{v}=-\overline{\nabla}\times\overline{\nabla}\times\overline{v}+\overline{\nabla}\left(\overline{\nabla}\cdot\overline{v}\right)$ and applying the continuity equation for incompressible flow $\overline{\nabla}\cdot\overline{v}=0$.[9] For fully developed flow $\frac{\partial P_i^*}{\partial\theta}$ must be independent of θ. Further on differentiating Eqs. 5 and Eq. 6 with respect to θ and imposing the condition of a fully developed velocity field one obtains $\frac{\partial^2 P_i^*}{\partial\eta\partial\theta}=\frac{\partial^2 P_i^*}{\partial r\partial\theta}=0$. Thus $\frac{\partial P_i^*}{\partial\theta}$ is constant everywhere in the channel. However, the pressure gradient along any θ coordinate line (curves of constant r and η), i.e., $\frac{1}{(\zeta+r^*\sin\eta)}\frac{\partial P_i^*}{\partial\theta}$ varies inversely as the radius of curvature of that line.

Twelve boundary conditions are required to completely determine the velocity field. The core fluid's velocity should be bounded at $r=0$. For the annular fluid, the no-slip condition is applicable at the channel wall

$$\left.\begin{aligned}\{u_1;v_1;w_1\}&:\textit{bounded}\quad at\quad r=0\\ \{u_2;v_2;w_2\}&=0\qquad\quad at\quad r=1\end{aligned}\right\} \tag{8}$$

The remaining six boundary conditions are applied at the fluid interface ($r=k$). First, we impose conditions on the velocity at the interface. The normal component of the velocity must be zero as the interface is stationary. So $\overline{v}_1\cdot\overline{n}=\overline{v}_2\cdot\overline{n}$ at $r=k$, where $\overline{n}$ is the unit normal vector to the interface. Since the interface is circular and concentric with the channel wall (cf. Figure 1), we have

$$u_1=u_2=0\quad at\quad r=k \tag{9}$$

In this study, we are primarily concerned with liquid-liquid core-annular flows. Thus, continuity of the velocity field is imposed at the interface. This yields

$$\{v_1;w_1\}=\left(\frac{\mu_1}{\mu_2}\right)\{v_2;w_2\}\quad at\quad r=k \tag{10}$$

The viscosity ratio arises in the aforementioned equation because different velocity scales have been used for the core and annular fluids; each scale is based on the respective fluid's viscosity (cf. Eq. 2).

The final two conditions required to complete the problem are obtained by a balance of tangential stresses at the interface

$$\left.\begin{aligned}&\sigma_{r\eta,1}=\sigma_{r\eta,2}\quad at\quad r=k\\ &\frac{1}{k}\frac{\partial u_1}{\partial\eta}-\frac{v_1}{k}+\frac{\partial v_1}{\partial r}=\frac{1}{k}\frac{\partial u_2}{\partial\eta}-\frac{v_2}{k}+\frac{\partial v_2}{\partial r}\quad at\quad r=k\end{aligned}\right\} \tag{11}$$

$$\left.\begin{aligned}&\sigma_{r\theta,1}=\sigma_{r\theta,2}\quad at\quad r=k\\ &\frac{\partial w_1}{\partial r}=\frac{\partial w_2}{\partial r}\quad at\quad r=k\end{aligned}\right\} \tag{12}$$

Since the location of the interface is known, the normal stress balance is not required to obtain the solution of the velocity field. However, for the solution to be physically valid, it must satisfy the normal stress balance. This is shown to be the case provided the physical parameters satisfy a condition which is derived later (Eq. 37).

On setting $\varepsilon=0$, the aforementioned equations describe CA flow in a straight channel, in a cylindrical coordinate system. For the case of a curved channel ($\varepsilon\neq0$), the governing equations are highly nonlinear and coupled. Considering the problem in the asymptotic limit of a gently curved channel ($\varepsilon\ll1$) allows the derivation of an approximate analytical solution. This is carried out in the next section.

Asymptotic solution for a gently curved channel to $O(\varepsilon^1)$

A regular perturbation analysis of the nonlinear governing equations results in a series of linear problems which may be solved successively. A solution in the form of an asymptotic power series in ε is assumed for all variables. Here, the first subscript denotes the fluid and the second subscript denotes the term in the asymptotic expansion

$$\left.\begin{aligned}u_i&=u_{i,0}+u_{i,1}\varepsilon+O(\varepsilon^2)\\ v_i&=v_{i,0}+v_{i,1}\varepsilon+O(\varepsilon^2)\\ w_i&=w_{i,0}+w_{i,1}\varepsilon+O(\varepsilon^2)\\ P_i&=P_{i,0}+P_{i,1}\varepsilon+O(\varepsilon^2)\end{aligned}\right\} \tag{13}$$

The expansions in Eq. 13 are substituted into the governing equations and boundary conditions. Since ε is arbitrary, the coefficients of every power of ε in the resulting equations and boundary conditions must be identically zero for Eq. 13 to be a solution. This procedure yields a hierarchy of linear problems which are solved in succession.[21]

The problem at $O(\varepsilon^0)$ is the case of $\varepsilon=0$ which corresponds to fully developed CA flow in a straight channel. The solution of this problem is straightforward and well known. It is given in Eq.14. There is no flow in the radial and azimuthal directions. The axial velocity profile is axisymmetric with the maximum at the center of the channel. The pressure gradient is constant throughout the domain and equals the pressure gradient along the centerline of the curved channel (G)

$$\left.\begin{aligned} &u_{i,0}=v_{i,0}=0 \\ &w_{1,0}=\frac{1}{4}\left[k^2+\frac{\mu_1}{\mu_2}\left(1-k^2\right)-r^2\right] \quad r<k \\ &w_{2,0}=\frac{1}{4}\left[1-r^2\right] \quad k\le r\le 1 \end{aligned}\right\} \tag{14}$$

The governing equations at $O(\varepsilon^1)$ are

$$\frac{\partial u_{i,1}}{\partial r}+\frac{u_{i,1}}{r}+\frac{1}{r}\frac{\partial v_{i,1}}{\partial \eta}=0 \tag{15}$$

$$-\mathrm{Re}_i {w_{i,0}}^2\sin\eta=-\frac{\partial P_{i,1}}{\partial r}-\frac{1}{r}\frac{\partial}{\partial \eta}\left(\frac{\partial v_{i,1}}{\partial r}+\frac{v_{i,1}}{r}-\frac{1}{r}\frac{\partial u_{i,1}}{\partial \eta}\right) \tag{16}$$

$$-\mathrm{Re}_i {w_{i,0}}^2\cos\eta=-\frac{1}{r}\frac{\partial P_{i,1}}{\partial \eta}+\frac{\partial}{\partial r}\left(\frac{\partial v_{i,1}}{\partial r}+\frac{v_{i,1}}{r}-\frac{1}{r}\frac{\partial u_{i,1}}{\partial \eta}\right) \tag{17}$$

$$\mathrm{Re}_i u_{i,1}\frac{\partial w_{i,0}}{\partial r}=-r\sin\eta+\left(\frac{\partial}{\partial r}+\frac{1}{r}\right)\left(\frac{\partial w_{i,1}}{\partial r}+w_{i,0}\sin\eta\right)+\frac{1}{r}\frac{\partial}{\partial \eta}\left(\frac{1}{r}\frac{\partial w_{i,1}}{\partial \eta}+w_{i,0}\cos\eta\right) \tag{18}$$

or

$$\left(\mathrm{Re}_i u_{i,1}-\sin\eta\right)\frac{\partial w_{i,0}}{\partial r}+r\sin\eta=\nabla^2\left(w_{i,1}\right)$$

where

$$\nabla^2=\left(\frac{\partial^2}{\partial r^2}+\frac{1}{r}\frac{\partial}{\partial r}+\frac{1}{r^2}\frac{\partial^2}{\partial \eta^2}\right) \tag{19}$$

The boundary conditions for the first-order problem are

$$\left.\begin{aligned} &\left\{u_{1,1};v_{1,1};w_{1,1}\right\}: bounded \quad at \quad r=0 \\ &\left\{u_{2,1};v_{2,1};w_{2,1}\right\}=0 \quad at \quad r=1 \end{aligned}\right\} \tag{20}$$

$$\left\{v_{1,1};w_{1,1}\right\}=\left(\frac{\mu_1}{\mu_2}\right)\left\{v_{2,1};w_{2,1}\right\} \quad at \quad r=k \tag{21}$$

$$u_{1,1}=u_{2,1}=0 \quad at \quad r=k \tag{22}$$

$$\frac{1}{k}\frac{\partial u_{1,1}}{\partial \eta}-\frac{v_{1,1}}{k}+\frac{\partial v_{1,1}}{\partial r}=\frac{1}{k}\frac{\partial u_{2,1}}{\partial \eta}-\frac{v_{2,1}}{k}+\frac{\partial v_{2,1}}{\partial r} \quad at \quad r=k \tag{23}$$

$$\frac{\partial w_{1,1}}{\partial r}=\frac{\partial w_{2,1}}{\partial r} \quad at \quad r=k \tag{24}$$

The centrifugal force is accounted for by the nonhomogeneous terms on the lefthand side of Eqs. 16 and 17. These equations do not admit a trivial solution, and, therefore, the transverse velocity components are nonzero and a cross-channel flow will exist. Since $w_{i,0}$ is known, the problem is linear and may be solved analytically. The equations for $u_{i,1}$ and $v_{i,1}$, i.e., Eqs. 15–17 along with the corresponding boundary conditions are independent of $w_{i,1}$. Hence, they are first solved for $u_{i,1}$ and $v_{i,1}$, after which the solution for $w_{i,1}$ may be obtained. Based on Eq. 15 we define a "secondary stream function" which ensures that the equation of continuity (Eq. 15) is satisfied to first order in ε

$$u_{i,1}=-\frac{1}{r}\frac{\partial \psi_{i,1}}{\partial \eta}; \quad v_{i,1}=\frac{\partial \psi_{i,1}}{\partial r} \tag{25}$$

Substituting Eq. 25 into Eqs. 16 and 17, and eliminating the pressure gradient terms, one obtains

$$-2\mathrm{Re}_i w_{i,0}\cos\eta\frac{dw_{i,0}}{dr}=\nabla^2\left(\nabla^2\left(\psi_{i,1}\right)\right) \tag{26}$$

where ∇^2 is defined in Eq.19.

The solution is assumed to have a separable form $\psi_{i,1}=\overline{\psi}_{i,1}(r)\cos\eta$. Substituting in Eq. 26 one obtains the following fourth-order ordinary differential equation

$$-2\mathrm{Re}_i w_{i,0}\frac{dw_{i,0}}{dr}=D^2\left(D^2\left(\overline{\psi}_{i,1}\right)\right) \tag{27}$$

where

$$D^2\varphi=\left(\frac{d^2}{dr^2}+\frac{1}{r}\frac{d}{dr}-\frac{1}{r^2}\right)\varphi=\frac{d}{dr}\left(\frac{1}{r}\frac{d}{dr}(r\varphi)\right) \tag{28}$$

Equation 27 can be solved by direct integration to obtain the general solution in the domain of each fluid as given in the following

$$\left.\begin{aligned} \psi_{1,1}&=\cos\eta\left[\frac{F_1}{r}+\frac{B_1}{2}r\log(r)+r\left(\frac{C_1}{2}-\frac{B_1}{4}\right)+A_1\frac{r^3}{16}+\mathrm{Re}_1\frac{r^5}{768}\left(k^2+\frac{\mu_1}{\mu_2}\left(1-k^2\right)\right)-\mathrm{Re}_1\frac{r^7}{4608}\right] \\ \psi_{2,1}&=\cos\eta\left[\frac{F_2}{r}+\frac{B_2}{2}r\log(r)+r\left(\frac{C_2}{2}-\frac{B_2}{4}\right)+A_2\frac{r^3}{16}+\mathrm{Re}_2\frac{r^5}{768}-\mathrm{Re}_2\frac{r^7}{4608}\right] \end{aligned}\right\} \tag{29}$$

A_i, B_i, C_i and F_i are constants of integration. The general solution for the $u_{i,1}$ and $v_{i,1}$ velocity components may be obtained by substituting the aforementioned expressions into Eq. 25. The unknown constants are determined by applying the boundary conditions in Eqs. 20–23. This results in eight linear algebraic equations which are solved for the unknown constants to determine $\psi_{i,1}$, and, hence, $u_{i,1}$ and $v_{i,1}$. All the integration constants turn out to be multiples of either Re_1 or Re_2. Thus a circulatory flow will always exist in a curved channel ($\varepsilon\neq 0$). This is in contrast to the pressure driven flow between two infinite cylinders, where purely axial flow is possible because of the infinite vertical extent of the concentric cylinders. This axial flow is stable upto a critical Reynolds number. Beyond this, the flow becomes unstable and circulations arise.[22–24]

Next we turn to the solution of the axial velocity field. Equation 18 for $w_{i,1}$ is solved assuming a solution of the form $w_{i,1}=\overline{w}_{i,1}(r)\sin\eta$. Direct integration results in the following solution

$$w_{i,1}=\sin\eta\left[\frac{E_i}{r}+\frac{G_i r}{2}+\frac{3r^3}{16}-\frac{\mathrm{Re}_i}{16}r^3 u_{i,1}\right] \tag{30}$$

E_i and G_i are integration constants which are determined by application of the boundary conditions Eqs. 20, 21 and 24. The calculations have been carried out in Wolfram

Mathematica 8. The expressions for the constants are involved and are given in the supplementary material.

The solution for the velocity field to $O(\varepsilon^1)$ is given by substituting the solutions at zeroth and first-order into Eq.13

$$\left.\begin{aligned} u_i &= u_{i,1}\varepsilon \\ v_i &= v_{i,1}\varepsilon \\ w_i &= w_{i,0} + w_{i,1}\varepsilon \end{aligned}\right\} \tag{31}$$

In most experimental and numerical studies on flow in curved channels, the Dean number (De) is used as a key parameter. This parameter was first introduced by Dean[10] in his analysis of the flow rate of a single fluid through a curved channel. This parameter as defined by Dean is $\mathrm{De} = \varepsilon\ \mathrm{Re}^2$. However, in this work, we use the Reynolds numbers of each fluid and the curvature ratio (ε) as individual parameters. The curvature ratio (ε) effects the flow field as a separate parameter, independent of the Dean number. Separating this dependence is particularly important when studying the local features of the axial velocity. The constants of integration (E_i and G_i) in Eq.30 contain terms which are independent of the Reynolds numbers. Moreover, the third term of Eq. 30 is independent of $\mathrm{Re_i}$ and will appear in the final result for w_i (Eq. 31) as a term with dependence on ε alone. This term accounts for an important geometric effect of the channel's axial curvature on the axial velocity profile which will be discussed in more detail later. Furthermore, the Reynolds numbers and the curvature ratio account for fundamentally different properties of the system, especially in the case of two-phase flow. The Reynolds numbers of the two fluids may differ as they can have different transport properties. On the other hand, the curvature ratio is the same for both, as it is a geometric property of the channel.

The asymptotic solution is not valid for arbitrarily high Reynolds numbers. For the solution to be valid $\varepsilon w_{\mathrm{i},1} \ll w_{\mathrm{i},0}$. While $w_{\mathrm{i},0}$ is independent of the Reynolds numbers, the magnitude of $w_{\mathrm{i},1}$ increases with $\mathrm{Re_i}$. Thus, even for small values of the curvature ratio (ε) the first-order term can become large at sufficiently high $\mathrm{Re_i}$. A conservative upper limit on $\mathrm{Re_i}$ for the validity of the solution at small ε can be estimated by requiring $\frac{|w_{i,1}|}{|w_{i,0}|} \leq O(1)$. For moderate fractional core radii ($k \approx 0.5$), this condition is satisfied for Reynolds numbers upto 600. At extreme values of k, the upper limit on $\mathrm{Re_i}$ reduces to about 200. These estimates are applicable for a wide range of viscosity ratios from 0.1 to 5.

In the next section, we account for the balance of normal stresses at the circular, concentric interface and obtain a condition on the physical parameters for the circular concentric core solution to be valid.

Balance of Normal Stresses at the Circular Concentric Interface- Validity of the Solution

Here we show that the asymptotic solution (Eq. 29) does in fact satisfy the normal stress balance provided the physical parameters follow a certain constraint. This constraint on the parameter space is also derived below.

The normal stress balance in nondimensional form is given by

$$p_1 - p_2 + \overline{n}\ \cdot \overline{n} \cdot \overline{\overline{\sigma}}_2 - \overline{n} \cdot \overline{n} \cdot \overline{\overline{\sigma}}_1 = \frac{1}{Ca}(\nabla \cdot \overline{n})$$

with

$$Ca = \frac{\mu_i w_{i,c}}{\gamma} = \frac{GR^2}{\gamma} \tag{32}$$

where $\overline{n}$ is the unit normal vector, $\overline{\overline{\sigma}}$ is the deviatoric stress tensor and γ is the surface tension. Ca is a dimensionless parameter called the capillary number.

Since the interface is circular and concentric with the channel, the normal vector is the radial unit vector and Eq. 33 in component form is

$$p_1 - p_2 + 2\left(\frac{\partial u_2}{\partial r} - \frac{\partial u_1}{\partial r}\right) = \frac{1}{Ca}\left[\frac{1}{k} + \varepsilon\frac{\sin\eta}{(1+\varepsilon r\sin\eta)}\right] \tag{33}$$

This equation is applicable at $r = k$. To $O(\varepsilon^0)$, Eq. 33 is simply the Young-Laplace pressure jump condition for a cylinder

$$p_{1,0} - p_{2,0} = \frac{1}{Ca}\left[\frac{1}{k}\right] \tag{34}$$

The condition at $O(\varepsilon^1)$ is given below

$$p_{1,1} - p_{2,1} + 2\left(\frac{\partial u_{2,1}}{\partial r} - \frac{\partial u_{1,1}}{\partial r}\right) = \frac{1}{Ca}(\sin\eta) \tag{35}$$

The $\sin\eta$ term on the RHS of the equation is a nonhomogeneous forcing term which arises due to the curved nature of the channel. This term must be balanced for all η by the pressure and the viscous normal forces acting across the interface (lefthand side of Eq. 35) for the fully developed solution with a circular, concentric interface to be valid. The solution of the velocity field (Eqs. 29) has the following form

$$\begin{aligned} u_{i,1} &= \hat{u}_{i,1}(r)\sin\eta \\ v_{i,1} &= \hat{v}_{i,1}(r)\cos\eta \\ p_{i,1} &= \hat{p}_{i,1}(r)\sin\eta \end{aligned} \tag{36}$$

Substituting Eq. 36 in Eq.35 one finds that $\sin\eta$ may be eliminated from both sides of the equation, and one is left with a constraint on the physical parameters of the following form

$$\Phi\left(\mathrm{Re}_1, \mathrm{Re}_2, \frac{\mu_1}{\mu_2}, k\right) = \frac{1}{Ca} \tag{37}$$

Equation 37 establishes a condition on the adjustable physical flow parameters (G, R, k) in terms of the fluid properties $[\rho_1, \rho_2, (\mu_1/\mu_2)]$, which must be satisfied if one is to have a fully developed solution with a circular concentric core. The complete expression for Eq. 37 is lengthy and is available in the supplementary material. It is obtained by first eliminating pressure from Eq. 35 using the momentum equation in the η direction. The resultant expression may be evaluated using the solution for the velocity field. If one takes particular values for k and (μ_1/μ_2), a simple linear relationship is obtained between the Reynolds numbers and the capillary number (Ca). For example, with $k = 0.5$ and $(\mu_1/\mu_2) = 2$ one obtains to the fourth decimal

$$\mathrm{Re}_1 = 11.7133\frac{1}{Ca} + 0.0543\mathrm{Re}_2 \tag{38}$$

Interestingly, if the Ca is sufficiently small, then the critical Reynolds number of the core fluid (Re_1) is practically independent of the Reynolds number of the annular fluid (Re_2).

It is important to note that Eq. 37 does *not* govern the *stability* of the CA flow. It is only a condition for the core to be concentric with the channel. Even when Eq. 37 is not

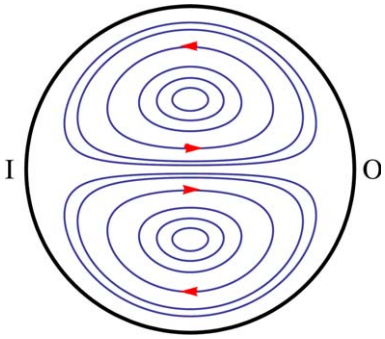

Figure 2. Secondary circulations in single-phase flow through a curved channel.[9]

(O) represents the outer side of the channel and (I) represents the inner side of the channel. [Color figure can be viewed in the online issue, which is available at wileyonlinelibrary.com.]

fulfilled, a stable CA flow can persist; although the core will be noncircular and displaced toward the walls. Such CA flows have been observed in the curved bends of microchannels.[3] This is discussed further in the Concluding Remarks section. In the sections that follow, we analyze two key features of the CA flow in a curved channel. These are the secondary circulations and the redistribution of the axial velocity.

Analysis of the Secondary Circulation Flow Structure

Types of circulation patterns: principle, sandwich and dominated vortices

As fluid flows in a curved channel, it experiences a centrifugal force which depends on the local axial velocity. In single-phase Poiseuille flow, the velocity is greater near the center of the channel and falls off to zero at the walls. The faster flowing fluid, near the center of the channel, experiences a greater centrifugal force. This sets up a transverse pressure gradient which induces circulations in the form of two counter rotating vortices. The fluid elements follow a spiral path, drifting across the cross section as they proceed along the channel length. The circulations may be visualized by projecting streamlines onto the cross sectional plane as presented in Figure 2. The fluid flows outwards along the horizontal centerline of the channel cross section and back inwards along the channel wall. In this study, the outer side of the channel is taken to be on the righthand side. Thus, the fluid in the (upper) lower half of the channel circulates in a (counter) clockwise fashion. These results were first presented theoretically by Dean.[9]

In this case of two-phase core-annular (CA) flow, the same physics is at work. Both the core and annular fluids will develop a secondary flow with counter-rotating vortices. However, the flow field exhibits rich features induced by the coupling of the fluids at the interface. This coupling is inherent in the mathematical equations via the boundary conditions which enforce continuity of velocity and equality of shear stresses (Eqs.21–24). The secondary flow structure at $O(\varepsilon^1)$ may be conveniently visualized by plotting contours of the secondary streamfunction $\psi_{i,1}$ (Eqs. 25 and 29). These curves are equivalent to projections of the three-dimensional streamlines onto the r - η plane. The projected streamlines at $O(\varepsilon^1)$ are independent of the curvature ratio (ε). Variations in ε effect the intensity of the transverse flow, but not the circulation pattern, in the limit of small ε (cf. Eq. 31).

In analogy with the single-phase flows studied by Dean,[9] one may anticipate a pair of counter-rotating vortices in each fluid. This situation is depicted in Figure 3. The vortices in the annular fluid are C-shaped. Both vortex pairs have the same natural direction of circulation as in a single-phase flow. Specifically, fluid in the (upper) lower half of the channel circulates in a (counter) clockwise fashion. These vortices are called "principle vortices". Since the fluid on either side of the interface flows in opposite directions, the velocity must be identically zero at the interface, to maintain continuity of the velocity field. These observations are confirmed by a plot of the η component of velocity along the vertical centerline $v_{i,1}(r,\ \eta = 0)$ (cf. Figure 3). A positive $v_{i,1}$ indicates flow toward the outer side of the channel which is on the right of the figure. The velocity changes sign across the interface and is exactly zero at the interface. The function $v_{i,1}(r,\ \eta = 0)$ goes to zero once within each of the fluids, apart from satisfying the no-slip condition at $r = 1$. These zeros correspond to the centers of the principle vortices in the upper half of the channel.

The case of two principle vortex pairs is a very special one. In general, the velocity will be nonzero at the interface.

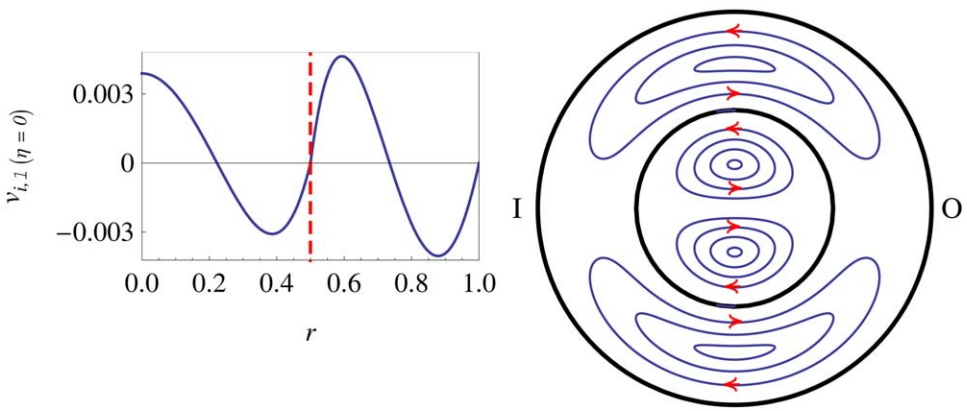

Figure 3. Two principle vortices.

Circulatory flow pattern for the case of $Re_1 = 30$, $Re_2 = 30$, $(\mu_1/\mu_2) = 1.9$, $k = 0.5$. The interface location is indicated by the dashed (red) vertical line. (O) represents the outer side of the channel, and (I) represents the inner side of the channel. [Color figure can be viewed in the online issue, which is available at wileyonlinelibrary.com.]

In this case, a third pair of vortices are formed, which we call "sandwich vortices". These act as an intermediate between the principle vortices in each fluid, ensuring velocity continuity. It is instructive to think of the fluid which contains the sandwich vortex pairs as being influenced by the other fluid. At the interface, one fluids drags the other along with itself, causing the latter to flow against its natural tendency. The location of the sandwich vortex depends on the fluid properties and relative flow rates (which decide the radius of the core k). These arguments will now be made clearer by considering specific examples. The dependence of the circulation structure on the parameter space will be investigated in detail, after the various possible cases are presented.

In Figure 4, the annular fluid influences the core fluid. Consider the upper half of the channel cross section. A single counterclockwise principle vortex is present in the annular fluid. On the other hand, the core fluid contains two vortices. A counter clockwise principle vortex is present in the bulk, while a clockwise sandwich vortex is located near the interface. A part of the core fluid adjacent to the interface is dragged in a clockwise direction by the neighboring annular fluid. In the $v_{i,1}(r, \eta = 0)$ line plot, the velocity is not zero at the interface. Instead there are two zeros located in the core fluid ($r < k$). The zero at which the derivative is negative corresponds to the principle vortex center. The other zero at which the derivative is positive corresponds to the sandwich vortex center.

Figure 5 depicts the situation when the core fluid influences the annular fluid. Here, the sandwich vortex is located within the annular fluid. The circulation pattern consisting of only principle vortices (Figure 3) represents a transition between the flow regimes depicted in Figures 4 and 5. On the one side, the annular fluid influences the circulations in the core fluid while across this transition the core fluid influences the annular fluid.

As the influence of one fluid over another increases (on suitable variation of parameters) the sandwich vortex grows at the expense of the principle vortex. Ultimately, the principle vortex will disappear altogether, leaving behind the sandwich vortex. The sandwich vortex now occupies the entire domain. This is called a "dominated vortex". It corresponds to a complete reversal of the natural circulatory flow in a fluid under the viscous influence of the other fluid. In Figure 6, the natural circulation pattern of the core is reversed due to the drag exerted by the annular fluid. In structure, this flow looks similar to the case of two principle vortices (Figure 3), the critical difference being the direction of circulation in the core fluid. Figure 7 depicts the case when the circulation in the annular fluid is reversed.

Variation of the circulation pattern across parameter space

Now we study the variation of the circulatory flow in the 4-D parameter space Re_1, Re_2 (μ_1/μ_2) and k. This is accomplished by obtaining critical boundaries which divide the parameter space into regions corresponding to various flow patterns. We focus on the η component of velocity along the vertical centerline, $v_{i,1}(r, \eta = 0)$. The velocity must be zero at $r = 1$ according to the no-slip condition. Any other zero of the velocity function represents a vortex center, i.e. $v_{i,1}(r_o, 0) = 0$ implies a vortex center at $(r_o, 0)$, except for $r_o = 0$. About the vortex center the velocity is positive on one side and negative on the other. The derivative at the zero (r_o) indicates the nature of the vortex (principle or sandwich/dominated). We now derive relations for the critical boundaries between flow regimes in the parameter space. This is done by tracking the zeros of the velocity function, $v_{i,1}(r, \eta = 0)$.

The first critical boundary corresponds to the case when only principle vortices exist and the velocity is zero at the interface

$$v_{i,1}\left(r=k, \eta=0; \mathrm{Re}_1, \mathrm{Re}_2, \frac{\mu_1}{\mu_2}, k\right)=0 \tag{39}$$

When the sandwich vortex occupies a larger portion of a fluid, the principle vortex center shift toward the end point of the respective fluid domain, i.e., $r = 0$ for the core and $r = 1$ for the annulus. When the sandwich vortex occupies the entire fluid, becoming a dominated vortex, then the zero of $v_{i,1}(r, \eta = 0)$ corresponding to the principle vortex must vanish. This provides two critical conditions. In the case of the core fluid $v_{i,1}(r, \eta = 0)$ will be zero exactly at $r = 0$

$$v_{1,1}\left(r=0, \eta=0; \mathrm{Re}_1, \mathrm{Re}_2, \frac{\mu_1}{\mu_2}, k\right)=0 \tag{40}$$

The approach to the transition, as the viscosity ratio is decreased, is illustrated in Figure 8a. Beyond this transition, there will be only one zero in the core fluid which corresponds to the dominated vortex (Figure 6).

As the transition to a dominated vortex in the annular fluid is approached, the zero corresponding to the principle vortex migrates toward $r = 1$. However, $v_{i,1}(r, \eta = 0)$ is always zero at $r = 1$, due to the no-slip condition. Hence at the critical transition point, two zeros must merge at $r = 1$, which leads to a zero derivative condition

$$\frac{dv_{2,1}}{dr}\left(r, \eta=0; \mathrm{Re}_1, \mathrm{Re}_2, \frac{\mu_1}{\mu_2}, k\right)=0 \quad at \quad r=1 \tag{41}$$

The velocity profiles as this critical tangency condition is approached are presented in Figure 8b. Here, the viscosity ratio is increased to cause this transition beyond which the core fluid dominates the annular fluid (Figure 7).

Each of the three critical conditions (Eqs. 39–41) are solved for (μ_1/μ_2). This results in a family of critical curves in the $[k, (\mu_1/\mu_2)]$ plane which are parameterized by Re_1 and Re_2. These curves delineate the $[k, (\mu_1/\mu_2)]$ parameter space into four regions, each with a characteristic circulation pattern. Three such circulation flow regime maps are presented in Figure 9 for various combinations of Reynolds numbers. Consider the case of equal Reynolds numbers, specifically $\mathrm{Re}_1 = 30$ and $\mathrm{Re}_2 = 30$ (Figure 9b). On the extreme right, at large core radii, the core dominates the annular fluid. Here, the annular fluid circulates in a clockwise manner in the upper half of the cross section, contrary to its natural flow tendency. On the extreme left at low core radii, the annular fluid dominates the core fluid which now contains the dominated vortex. Both these regions are bounded by the critical curves of Eqs. 40 and 41 represented by solid lines. Just across these curves lie the two regions where the sandwich vortices exist along with principle vortices. These two regions are divided by the critical curve of Eq. 39, represented by the dashed line. Along this line only principle votices exist in the flow. On the left of this transition, the sandwich vortex lies in the core fluid, while on the right, the sandwich vortex lies in the annular fluid.

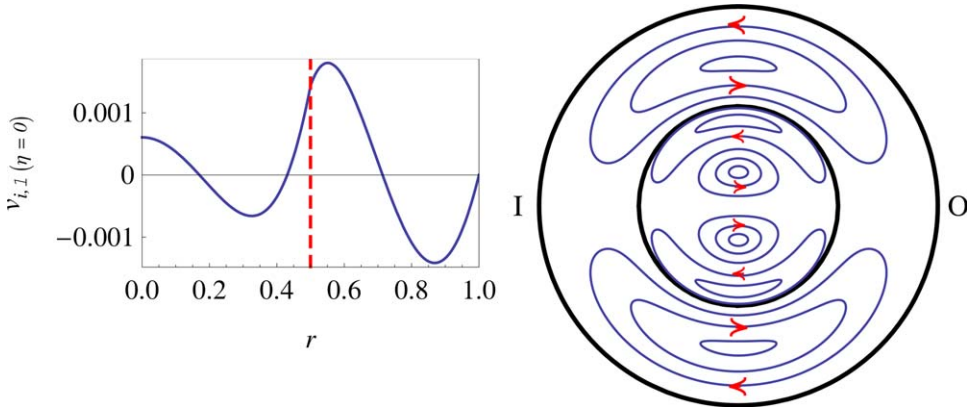

Figure 4. Sandwich vortex located in the core fluid.

Circulatory flow pattern for the case of $Re_1 = 30$, $Re_2 = 30$, $(\mu_1/\mu_2) = 0.5$, $k = 0.5$. [Color figure can be viewed in the online issue, which is available at wileyonlinelibrary.com.]

The fractional core radius quantifies the extent of the channel occupied by either fluid. The Reynolds numbers are defined using the radius of the channel (R) as a common length scale. Thus, a true indication of the relative strength of the centrifugal force, in comparison to viscous forces, in the core and annular fluid is given by Re_1k and $Re_2(1\text{-}k)$, respectively. Therefore, the fluid occupying a larger portion of the channel is able to dominate the circulatory flow, since the centrifugal force is relatively higher in that fluid. This is clearly observable in Figure 9. This is consistent with the fact that as one of the fluids occupies an increasingly large portion of the channel, the transverse flow in that fluid should approach the single-phase case.

At intermediate core radii, the circulation pattern is dependent on the viscosity ratio. The critical curve bounding the region in which the core fluid dominates (region I in Figure 9) varies monotonically with (μ_1/μ_2). Thus, while at low-core fluid viscosities a sandwich vortex may be present in the core, at higher core viscosities the sandwich vortex shifts to the annular fluid and ultimately the core can dominate the annular fluid completely. In contrast, the region in which the annular fluid dominates (region II in Figure 9) is bounded by a transition curve with a *turning point*. This is due to two opposing effects of having an annular fluid of relatively high viscosity (low viscosity ratios). For viscosity ratios greater than unity, the predominant result of decreasing the viscosity ratio is an increased influence of the annular fluid on the core fluid via interfacial viscous drag. However, for significantly more viscous annular fluids (viscosity ratios below unity), the viscous drag at the wall of the channel becomes significant and lowers the axial velocity. This in turn decreases the circulation intensity within the annular fluid. Thus even a high-viscosity annular fluid can be influenced by a lower viscosity core provided the core is not too small.

The effect of the fluids' densities may be understood by comparing the cases for different Reynolds numbers in Figure 9. The magnitude of the centrifugal force acting on a fluid is proportional to its density. In Figure 9a, $Re_1 < Re_2$ and region (II) in which the annular fluid dominates the core fluid enlarges. Alternatively, when $Re_1 > Re_2$, region (I) in which the core fluid dominates is relatively larger (Figure 9c).

The surface tension incorporated in the capillary number (Ca) does not affect the circulation pattern. However, for a circular, concentric core the Ca is not an independent parameter but rather is determined from Eq. 37 in terms of the other four parameters. When Ca is fixed, the parameter plane of Figure 9 is traversed along certain trajectories defined by Eq. 37. The trajectories for 3 values of Ca (10, 1, 0.2) are shown for the case of Figure 9b in Figure 10.

Intensity of the transverse flow and its dependence on the circulation pattern

Next the intensity of the transverse flow is investigated. Due to the competing nature of the transverse flow in each

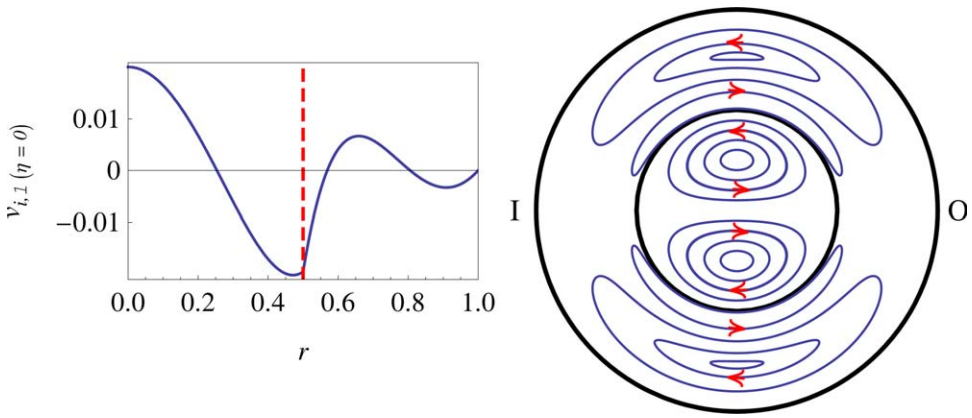

Figure 5. Sandwich vortex located in the annular fluid.

Circulatory flow pattern for the case of $Re_1 = 30$, $Re_2 = 20$, $(\mu_1/\mu_2) = 5.4$, $k = 0.5$. [Color figure can be viewed in the online issue, which is available at wileyonlinelibrary.com.]

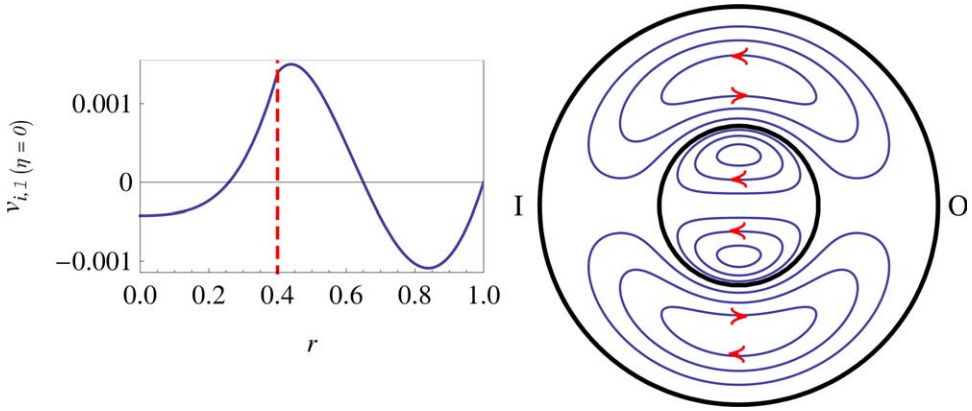

Figure 6. Annular fluid dominating the core fluid.

Circulatory flow pattern for the case of $Re_1 = 30$, $Re_2 = 30$, $(\mu_1/\mu_2) = 0.2$, $k = 0.4$. [Color figure can be viewed in the online issue, which is available at wileyonlinelibrary.com.]

fluid, the circulation intensity is parameter dependent and closely linked to the direction of circulation. As a quantitative measure of the intensity of circulation, we introduce an intensity factor (I_i). The squared magnitude of the transverse point velocity is computed for each fluid phase. This is then averaged over the area occupied by each fluid in the cross section to yield the respective intensity factors

$$I_1 = \frac{\int_0^{2\pi}\int_0^{k} r\left(u_{1,1}^2 + v_{1,1}^2\right) dr d\eta}{k^2\pi}, \quad I_2 = \frac{\int_0^{2\pi}\int_k^{1} r\left(u_{2,1}^2 + v_{2,1}^2\right) dr d\eta}{(1-k^2)\pi} \tag{42}$$

In order to better understand the relation between the direction of circulation and the intensity, we focus on a case of equal Reynolds numbers and viscosities. Specifically, $Re_1 = 30$, $Re_2 = 30$ and $= 1$. The corresponding circulation patterns at different fractional core radii (k) are given in Figure 9b. The intensity factor in each fluid is plotted against k in Figure 11. The intensity of circulation in the core (annular) fluid is greater at high (low) core radii. This result in conjunction with Figure 5b implies that the intensity of circulation in a particular fluid is high when only principle vortices are present in that fluid. On the other hand, when a fluid is strongly influenced by the other, such that sandwich/dominated vortices are present, then the circulation intensity of that fluid is low. A local minima of the circulation intensity is attained for each fluid at a core radii which roughly corresponds to the disappearance of the principle vortex in that fluid. The dominated vortex which is left behind in the fluid circulates in the opposite direction to the orignial principle vortex, but with a much lower intensity. Beyond this minima, as the core radius is further decreased (increased) the intensity of the dominated vortex in the core (annular) fluid increases due to the increasing influence of the other fluid which is circulating at high intensity. When the volume fraction of a fluid is very low, the intensity of the circulation in that fluid decreases to very low values.

Having understood the dependence of circulation intensity on the circulation pattern, some other general conclusions may be drawn from Figure 11. First, in an overall sense, the intensity of circulation in the core fluid is greater than that in the annular fluid. This is due to the viscous drag experienced by the annular fluid at the walls of the channel. Second, the circulation intensity in CA two phase flow is less than that of single phase flow. This is due to the competing nature of the circulatory flow within each fluid in CA flow which leads to a net reduction in the circulation intensity. Using the solution by Dean,[9] the single-phase intensity factor is calculated to be 0.00015 and is plotted as a horizontal line in Figure 11. Finally, as expected, when the volume fraction of a fluid approaches unity the circulation intensity in that fluid tends to that of the single-phase flow.

Apart from the presence of secondary circulations, the axial flow profile (w_i) in a curved channel is also

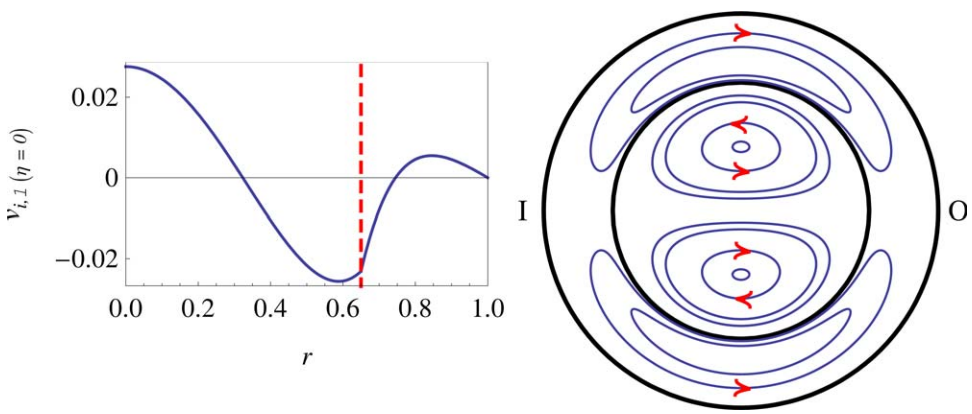

Figure 7. Core fluid dominating the annular fluid.

Circulatory flow pattern for the case of $Re_1 = 30$, $Re_2 = 30$, $(\mu_1/\mu_2) = 3.5$, $k = 0.65$. [Color figure can be viewed in the online issue, which is available at wileyonlinelibrary.com.]

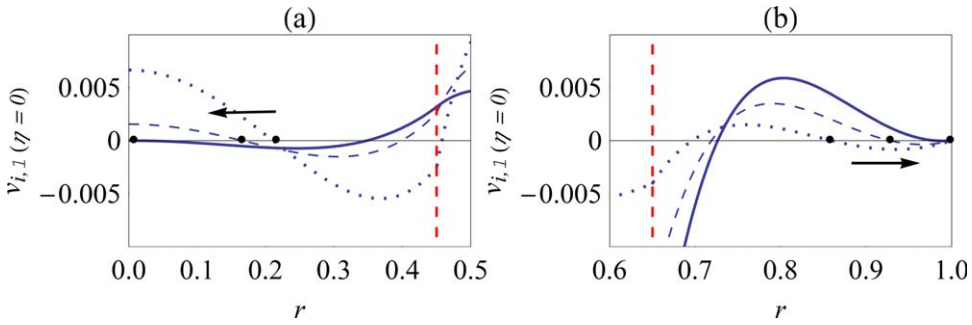

Figure 8. Examples of critical transition points.

(a) transition to annular fluid dominating the core fluid. Critical (Solid): $Re_1 = 30$, $Re_2 = 30$, $k = 0.45$ and $(\mu_1/\mu_2) = 1.08$; dashed: $(\mu_1/\mu_2) = 2.08$; dotted: $(\mu_1/\mu_2) = 4.08$, and (b) transition to core fluid dominating the annular fluid. Critical (Solid): $Re_1 = 10$, $Re_2 = 30$, $k = 0.65$ and $(\mu_1/\mu_2) = 8.7$; Dashed: $(\mu_1/\mu_2) = 6$; Dotted: $(\mu_1/\mu_2) = 3$. Only the relevant regions of the velocity profile are shown in each case. [Color figure can be viewed in the online issue, which is available at wileyonlinelibrary.com.]

qualitatively different from that in a straight channel. In the next two sections, we investigate this redistribution of the axial velocity.

Axial Velocity Redistribution in Single-Phase Flow

The symmetric axial velocity profile observed in a straight channel is redistributed when the channel is curved. The axial velocity in a curved channel is nonaxisymetric and the maximum is generally located off-center. The shift in the maximum can be either to the outer or the inner side of the channel. Although most studies report only the former behavior,[7,11] the axial velocity redistribution is in fact parameter dependent. This behavior results from two competing effects of the axial curvature of the channel.[25,26] These are the *geometric* and *inertial effects*. First these mechanisms are understood in the context of single-phase flows. These are then extended to the more complex two-phase CA flow.

Consider a fully developed single-phase flow in a curved channel (cf. Figure 1). The *geometric* effect arises due to the curvature of the θ coordinate lines. These are curves of constant r and η. The length of these coordinate lines in a section of the channel $\Delta\theta$ is given by $\Delta\theta(\zeta + r^* \sin\eta)$. Clearly, these lines are shorter in the inner half of the channel wherein $-\pi < \eta < 0$. The geometric effect increases the axial velocity in the inner half of the channel. It manifests via the viscous transport of momentum and by modifying the axial pressure gradient.

Radial, viscous transport of axial momentum will occur from the center of the channel toward the walls. Due to shorter axial distances, the inner side of the channel will experience a higher increase in axial velocity as compared to the outer side. The contribution of viscous transport to the axial velocity redistribution arises as an additional driving force term at $O(\varepsilon^1)$. This term is $\frac{\partial w_{s,0}}{\partial r} \sin\eta$ (cf. Eq. 18) which augments the pressure gradient. Here, the subscript (s) denotes a single phase fluid. Since $\frac{\partial w_{s,0}}{\partial r} \leq 0$, this term is positive in the inner half of the channel thus increasing the axial velocity in the inner half.

The angular axial pressure gradient $\frac{dP^*}{d\theta}$, is constant and independent of position in the channel. However, the pressure gradient driving force, given by $\frac{1}{(\zeta + r^* \sin\eta)} \frac{dP^*}{d\theta}$ is greater in the inner half of the channel, where the θ coordinate lines are shorter. This causes the axial velocity to increase in the inner half of the channel.

This influence of the geometry of the curved channel on viscous momentum transport and the axial pressure gradient is referred to as the *geometric* effect. It has also been called the potential flow effect.[26] The geometric effect accounts for the velocity redistribution in stable tangential (no circulations) pressure driven flow between two coaxial cylinders of infinite extent. The velocity is greater in the inner half at all Reynolds numbers for which the tangential flow is stable.[24]

The opposing mechanism which tends to increase the velocity in the outer half of the channel is the *inertial* effect. This is caused by the transverse circulatory flow. The principle contributing term in the equations at $O(\varepsilon^1)$ is $\mathrm{Re}_s u_{s,1} \frac{\partial w_{s,0}}{\partial r}$

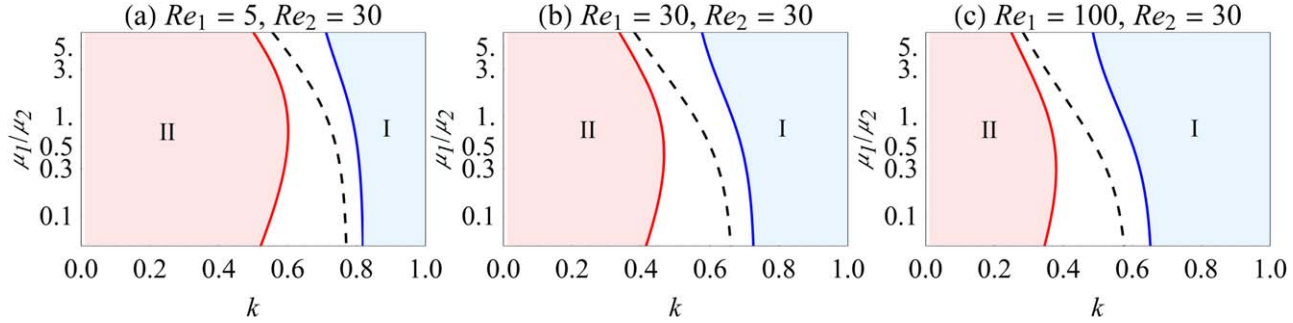

Figure 9. Circulatory flow regime map on the k - (μ_1/μ_2) plane at various Re_1 and Re_2.

(I) refers to the region in which the core fluid dominates and the dominated vortex is in the annular fluid, and (II) is the region in which the annular fluid dominates the core fluid. [Color figure can be viewed in the online issue, which is available at wileyonlinelibrary.com.]

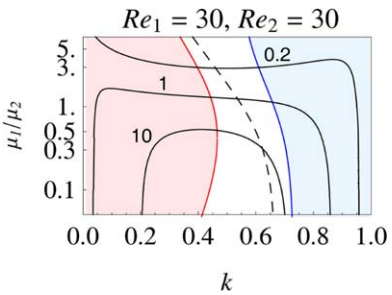

Figure 10. Trajectories of constant *Ca* (10, 1, 0.2) along which the parameter space may be crossed to satisfy Eq. 37 and ensure a circular, concentric interface.

[Color figure can be viewed in the online issue, which is available at wileyonlinelibrary.com.]

is (cf. Eq.18). The magnitude of this term increases with the Reynolds number which is indicative of the strength of the inertial forces. The circulatory flow transports fluid elements, near the horizontal centerline, from the inner wall to the outer wall of the channel. The axial velocity is lower near the wall and greater in the center of the channel. Hence, fluid near the horizontal centerline experiences a spatial acceleration in axial velocity followed by a deceleration as it flows across the channel. When the inertial forces are strong (high Re_s), the velocity continues to increase beyond the center of the channel ($r = 0$) and leads to a greater axial velocity in the outer half of the channel. Alternatively, one may interpret this phenomenon as a convective transport of axial momentum by the secondary circulations, toward the outer half of the channel.

The aforementioned reasoning is substantiated by considering Dean's asymptotic solution[9] to $O(\varepsilon^1)$ for the axial velocity of a single-fluid phase in a curved channel

$$\left.\begin{aligned} &w_s = w_{s,0} + w_{s,1}\varepsilon \\ &\textit{where} \\ &w_{s,0} = \frac{1}{4}\left(1-r^2\right) \\ &w_{s,1} = -r(1-r^2)\left(\frac{3}{16} + \mathrm{Re}_s^2 \frac{\left(-19+21r^2-9r^4+r^6\right)}{737280}\right)\sin\eta \end{aligned}\right\} \tag{43}$$

The aforementoined solution for the axial velocity consists of a modification ($w_{s,1}\varepsilon$) to the velocity profile in a straight pipe ($w_{s,0}$). The correction term ($w_{s,1}$) is antisymmetric about the vertical centerline, i.e.$\eta \in \{0, \pi\}$. Therefore, the axial velocity increases in one half of the channel and decreases in the other. The terms within the second set of parenthesis in Eq. 43 are of opposite sign. The constant term represents the geometric effect. The inertial effect is quantified by the second term which is proportional to the square of the Reynolds number (Re_s). When the Reynolds number (Re_s) is sufficiently high, $w_{s,1}$ will be positive in the outer half ($0 < \eta < \pi$), and negative in the inner half of the channel. Hence, at high Re_s, the axial velocity (w_s) is greater in the outer half. On the other hand, for lower Re_s, the geometric effect dominates and the velocity is greater in the inner half of the channel.

The relative simplicity of the single-phase problem allows one to directly examine the solution and obtain useful insights. This is not possible for the two-phase CA problem which has a more intricate solution. Thus, the insights obtained in this section are invaluable for understanding the axial velocity redistribution in CA flow which is investigated in the following section. Here, the geometric and inertial effects continue to play an important role, but are modified by additional influences of relative flow rates and viscous stress interaction at the fluid–fluid interface.

Analysis of the Axial Velocity Profile in Core-Annular Flow

Parameter dependent axial velocity redistribution

In two-phase CA annular flow, the *geometric* and *inertial* effects discussed above compete within each fluid phase to decide the axial velocity redistribution. The relative strength of the inertial forces depends on the respective Reynolds numbers and the fractional core radius (k). $k\ \mathrm{Re}_1$ and $(1\text{-}k)\ \mathrm{Re}_2$ are effective measures of the ratio of inertial to viscous forces in the core and annular fluids, respectively. Thus, depending on the parameters, the inertial effect may dominate in one fluid, while the geometric effect dominates in the other. Since the fluids are coupled at the interface, this leads to a range of velocity redistributions. Hence, the axial velocity profile at $O(\varepsilon^1)$ is dependent on the four parameters Re_1, Re_2 (μ_1/μ_2) and k. The curvature ratio (ε) does not effect the nature of the velocity redistribution at $O(\varepsilon^1)$. However, it does decide the extent by which the axial velocity is modified from the symmetric flow profile in a straight channel.

We focus on the horizontal centerline of the cross section where the velocity modification ($w_{i,1}$) is maximum, i.e. $\eta \in \{-\pi/2, \pi/2\}$. First consider the case when the Reynolds number of the core fluid is high, while that of the annular fluid is low. Here the *inertial* effect is suppressed in the annular fluid. Due to the geometric effect, the axial velocity in the annular fluid has a tendency to increase in the inner half of the channel. This will be the case for all core radii. However, in the core fluid, the inertial effect can overcome the geometric effect if the core is sufficiently large. Thus, while the axial velocity is greater on the inner side of the channel for small core sizes, this distribution of velocity will reverse for large core sizes. A series of transitions occur in the velocity profile as the core radius is varied from one

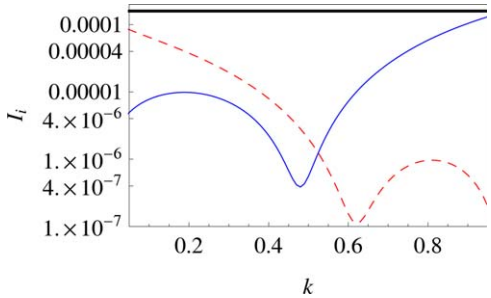

Figure 11. Semi-log plot of the intensity factor for circulations in each fluid phase for various fractional core radii (*k*).

Here, $\mathrm{Re}_1 = 30$, $\mathrm{Re}_2 = 30$ and $(\mu_1/\mu_2) = 1$. The solid (blue) line is the intensity factor in the core fluid (I_1) and the dashed (red) line is the intensity factor in the annular fluid (I_2). The solid (black) horizontal line is the intensity factor for single-phase flow. [Color figure can be viewed in the online issue, which is available at wileyonlinelibrary.com.]

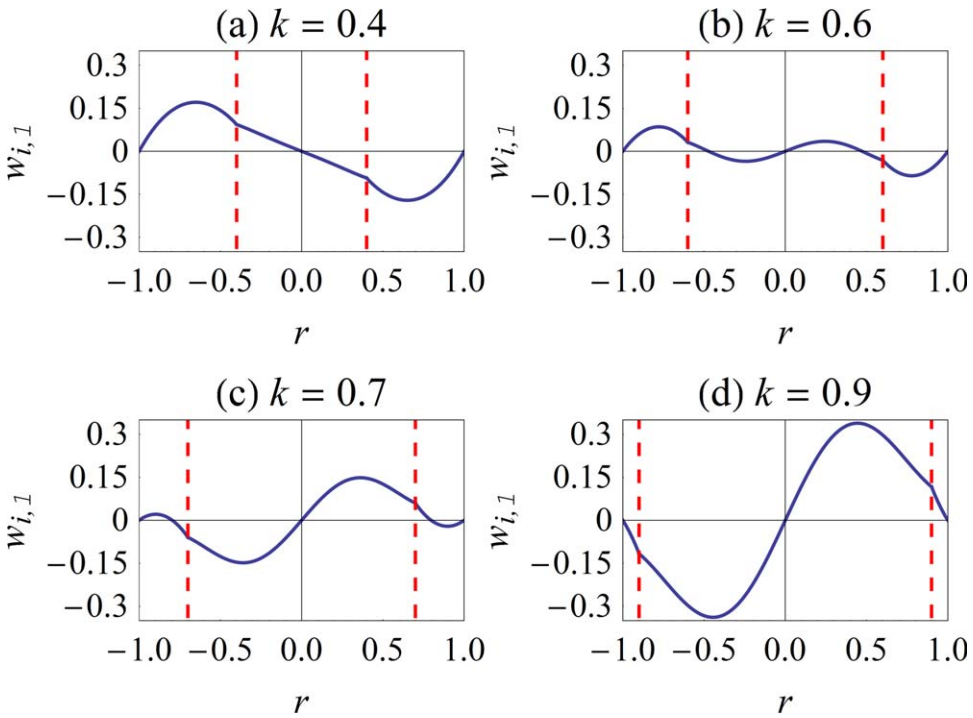

Figure 12. Profiles of the axial velocity correction term $w_{i,1}$ (cf. Eq. 31) at various core radii, for $Re_1 = 200$, $Re_2 = 10$ and $(\mu_1/\mu_2) = 3$.

Profiles are along the horizontal centreline of the cross section, i.e. $\eta \in \{-\pi/2, \pi/2\}$. The vertical dashed (red) line indicates the concentric interface of the fluids. Positive values of r indicate $\eta = \pi/2$ (outer half of the channel), while negative values indicate $\eta = -\pi/2$ (inner half of the channel). [Color figure can be viewed in the online issue, which is available at wileyonlinelibrary.com.]

extreme to the other. These are best understood by focusing on the axial velocity correction term $w_{i,1}$ (cf. Eq. 31).

In Figure 12, the $w_{i,1}$ profile is plotted at various core radii, for $Re_1 = 200$, $Re_2 = 10$ and $(\mu_1/\mu_2) = 3$. For small core radii, the axial velocity is clearly greater in the inner half of the channel as $w_{i,1}$ is everywhere positive on the inner side for both fluids (Figure 12a). The early signs of the increasing influence of the inertial effect is seen in Figure 12b, as part of the outer half of the core shows an increase in axial velocity. As the core radii gets larger and inertial forces become stronger, one reaches the point when the entire core has a greater axial velocity in the outer half. Due to a high-viscosity ratio ($(\mu_1/\mu_2) = 3$), the core is able to influence the velocity redistribution in the annular fluid as well (Figure 12c). Finally, at very large fractional core radii (Figure 12d), the velocity correction is everywhere positive in the outer half of the channel and the velocity distribution has reversed.

The axial velocity profiles ($w_{i,0} + \varepsilon\ w_{i,1}$) for $k = 0.4$ and $k = 0.9$ are plotted in Figure 13a and 13c, respectively. Enlarged and focused versions of these plots in Figure 13b and 13d clearly demonstrate the increase of axial velocity in the inner and outer halves of the channel, respectively. The increase of axial velocity on the inner side, caused by the geometric effect, is not very significant. Therefore, most experimental and numerical studies only report an increase of velocity in the outer half of the channel,[11,7] i.e., the inertial effect of a curved channel.

Next consider the opposite situation of a high Reynolds number of the annular fluid and a low Reynolds number of the core fluid. Here the inertial effect is suppressed in the core while it is able to dominate in the annulus for sufficiently small core radii. Moreover, if the viscosity ratio is small, the annular fluid can have a strong influence over the velocity profile in the core. Figure 14 depicts $w_{i,1}$ profiles at various core radii for $Re_1 = 10$, $Re_2 = 200$ and $(\mu_1/\mu_2) = 0.1$. As the core radius is decreased, a series of transitions, similar to those in Figure 12, are observed. At large fractional core radii (k), the *geometric* effect dominates throughout and the axial velocity correction is positive in the inner half of the channel (Figure 14a). As the core radius is decreased, the *inertial* effect comes into play in the annular fluid. Thus, one observes a region of positive velocity modification in the outer section of the annular fluid (Figure 14b). At smaller core radii, the core fluid shows a greater velocity in the outer half due to the influence of the annular fluid (Figure 14c). Ultimately for sufficiently small core radii, the axial velocity is greater in the outer half of the channel for both fluids (Figure 14d).

Variation of the velocity redistribution across parameter space

Now we study the parametric dependence of the velocity redistribution. A careful examination of Figure 12 and Figure 14 reveal three critical transitions. These prove invaluable in organizing the parameter space in terms of the axial velocity redistribution. One critical transition occurs when the $w_{1,1}$ profile has a point of inflection at the channel center, $r = 0$ (Figure 14b–d). This heralds a change in the velocity redistribution in the core. A similar zero derivative condition occurs at $r = 1$ for $w_{2,1}$ (Figure 14c–d). This indicates a change in the velocity redistribution in the annular fluid. The third critical condition occurs when the modification in axial velocity is zero at the interface (Figure 14a–b). This

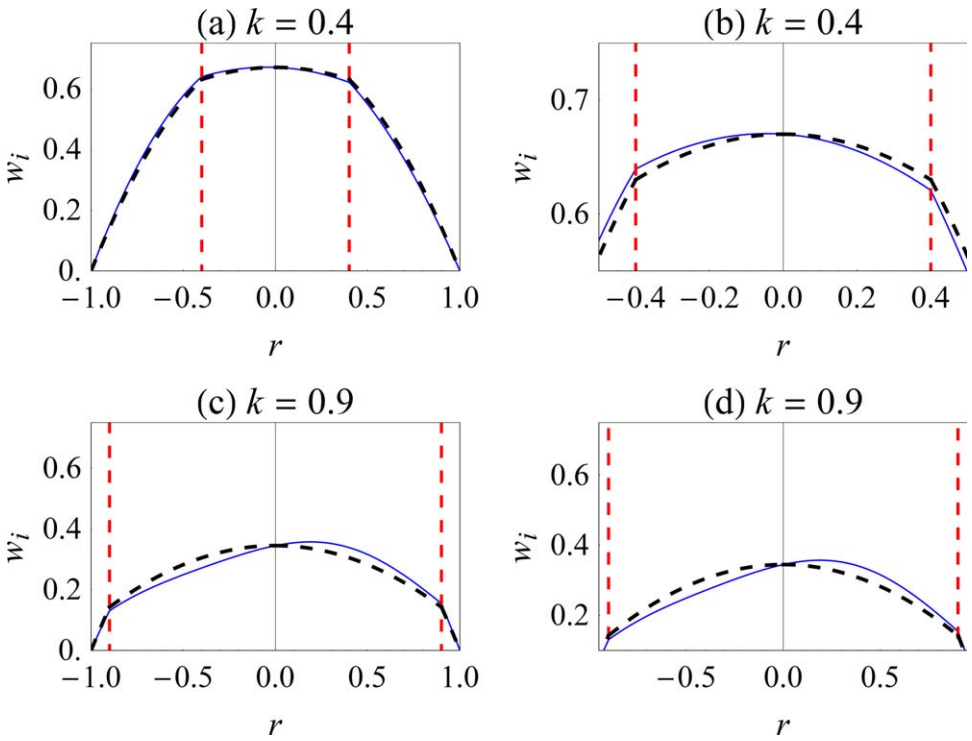

Figure 13. Profiles of the axial velocity at various core radii in a curved channel, for $Re_1 = 200$, $Re_2 = 10$ and $(\mu_1/\mu_2) = 3$.

The dashed (black) curve corresponds to flow in a straight channel. The region near the channel's centre in plots (a) and (c) are enlarged in (b) and (d), respectively. [Color figure can be viewed in the online issue, which is available at wileyonlinelibrary.com.]

corresponds to the case when both fluids have an opposite velocity redistribution. These conditions are stated in the following.

Condition for transition in the core fluid

$$\frac{dw_{1,1}}{dr}\left(r, \eta \in \left\{-\frac{\pi}{2}, \frac{\pi}{2}\right\}; \mathrm{Re}_1, \mathrm{Re}_2, \frac{\mu_1}{\mu_2}, k\right) = 0 \quad at \quad r = 0 \tag{44}$$

Condition for transition in the annular fluid

$$\frac{dw_{2,1}}{dr}\left(r, \eta \in \left\{-\frac{\pi}{2}, \frac{\pi}{2}\right\}; \mathrm{Re}_1, \mathrm{Re}_2, \frac{\mu_1}{\mu_2}, k\right) = 0 \quad at \quad r = 1 \tag{45}$$

Condition for an opposite axial velocity redistribution

$$w_{i,1}\left(r = k, \eta \in \left\{-\frac{\pi}{2}, \frac{\pi}{2}\right\}; \mathrm{Re}_1, \mathrm{Re}_2, \frac{\mu_1}{\mu_2}, k\right) = 0 \tag{46}$$

These conditions are used to obtain a family of curves in the $[k, (\mu_1/\mu_2)]$ parameter plane which are parameterized by Re_1 and Re_2. The results are presented in Figure 15 for three combinations of Re_1 and Re_2. In the first two cases (Figure 15a and b) the Reynolds numbers are chosen as in Figure 12 and Figure 14 in order to suppress the inertial effect in one of the fluids. In both these cases only three critical curves are present and the parameter plane is divided into four regions. The critical curves occur at large-core radii when Re_2 is small and at small core radii when Re_1 is small. The axial velocity modification ($w_{i,1}$) profile in each region of Figure 15a and Figure 15b is qualitatively the same as those presented in Figure 12 and Figure 14 respectively.

In the third case the Reynolds number of each fluids is given the same relatively high value of 200. The inertial effect is no longer suppressed and one obtains both sets of critical curves at high and low radii. In this sense, the behavior in Figure 15c is a combination of the two subcases in Figure 15a and Figure 15b. Six critical curves divide the parameter plane into 7 regions and the entire range of axial velocity redistribution profiles (Figure 12 and Figure 14) are possible.

In this section, it has been demonstrated that the axial velocity in a gently curved channel may be higher either on the outer or inner side of the channel. This redistribution from the symmetric axial velocity profile in a straight pipe depends on the parameter space in a nontrivial manner. A clear understanding of the underlying mechanisms has been possible by analyzing the asymptotic solution at $O(\varepsilon^1)$.

Motivation for Extending the Analysis to $O(\varepsilon^2)$

According to the solution at $O(\varepsilon^1)$, the flow rate through a curved channel is the same as that through a straight channel. The volumetric flow rate is a bulk property of the flow and is given by integrating the asymptotic solution for the axial velocity over the channel cross section. It is clear that the first-order term in Eq. 30 makes no contribution to the flow rate, since an integral of *sin* η over the cross section is zero. However, this is not the case for the second-order term. Therefore, the change in flow rate is an $O(\varepsilon^2)$ effect of the curvature.

In the case of single-phase flow, the solution at $O(\varepsilon^2)$ shows that the flow rate is less in a curved channel as

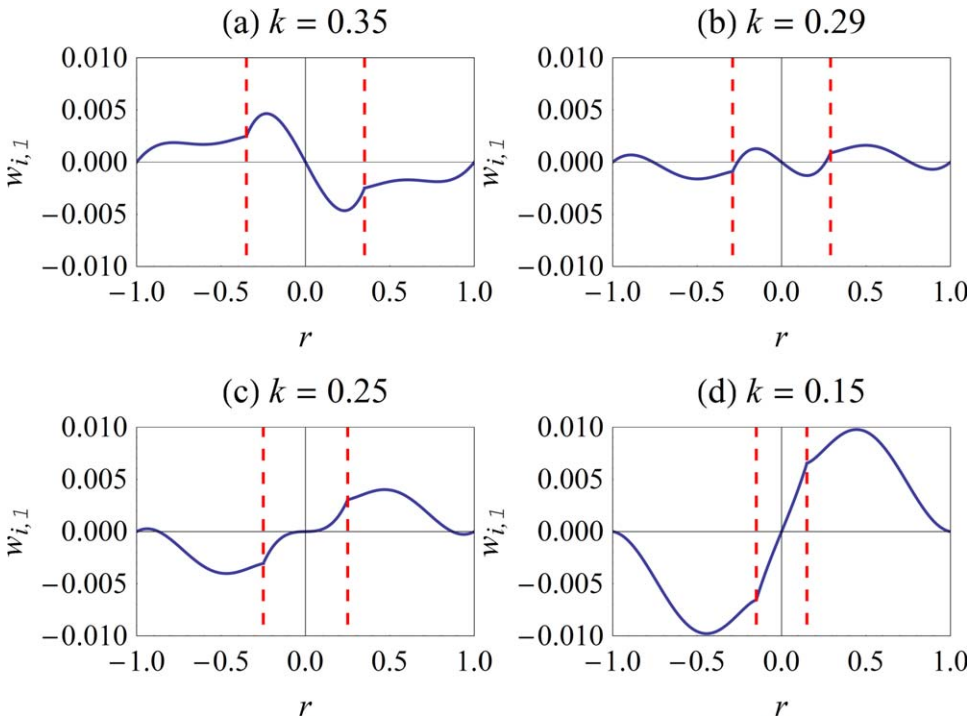

Figure 14. Profiles of the axial velocity correction term $w_{i,1}$ (cf. Eq. 31) at various core radii, for $Re_1 = 10$, $Re_2 = 200$ and $(\mu_1/\mu_2) = 0.1$.

[Color figure can be viewed in the online issue, which is available at wileyonlinelibrary.com.]

compared to a straight channel with the same centerline pressure gradient.[10] This is to be expected since a finite amount of energy is expended in driving the transverse flow in a curved channel. This is true of the core-annular flow as well. The reduction in the flow rate and its dependence on the system parameters will be a significant outcome of the second-order calculation.

Another qualitative feature which can only be captured at $O(\varepsilon^2)$ is the effect of the channel's curvature on the circulation flow pattern. Since the cross channel velocity

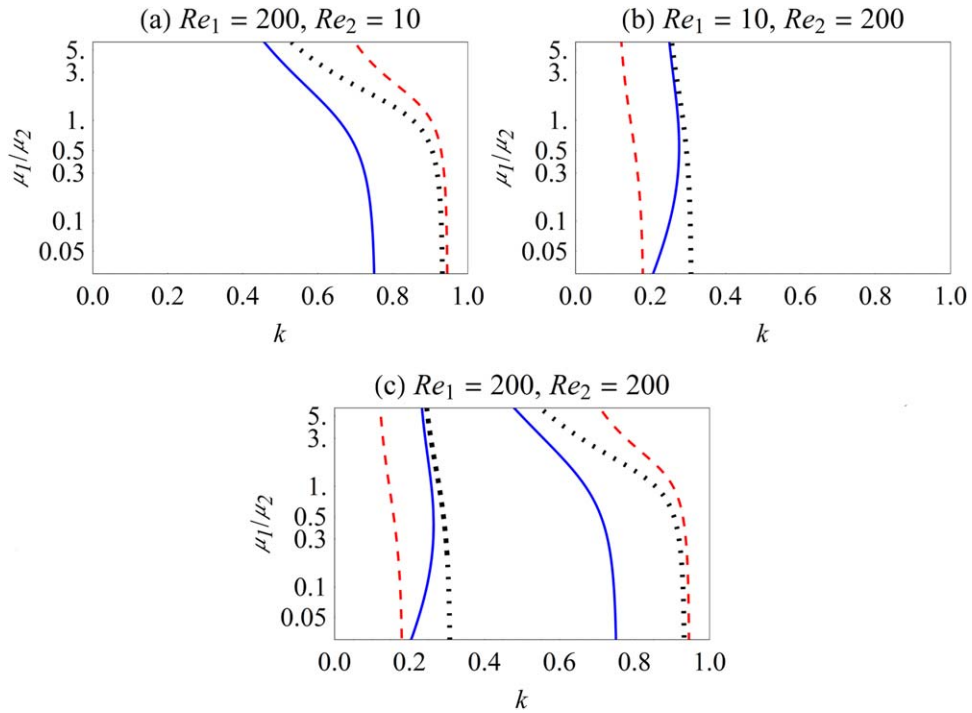

Figure 15. Parameter maps of the axial velocity distribution for various Reynolds number combinations.

Solid-blue line is the critical curve for transition in the core fluid Eq.44. Dashed-red line is the critical curve for transition in the annular fluid Eq. 45. The dotted black-line is the critical curve along which the core and annular fluids have an opposite velocity redistribution Eq. 46. [Color figure can be viewed in the online issue, which is available at wileyonlinelibrary.com.]

components at $O(\varepsilon^0)$ are zero in Eq. 31, ε effects only the magnitude of the velocity and not its spatial variation. Thus it can affect the intensity of the circulations but not their structure. However, at $O(\varepsilon^2)$ the velocity will be given by the sum of the first and second-order terms of the asymptotic expansion, both of which have different functional forms. The relative contribution of each term to the solution would depend on ε. Therefore, the circulation structure would be dependent on the curvature ratio at $O(\varepsilon^2)$. This discussion holds true for the effect of ε on the nature of the axial velocity redistribution as well.

Of course for sufficiently small ε the second-order term will be negligible. Thus, for a gently curved channel, small variations in the curvature ratio do not affect the velocity field significantly. However, beyond this asymptotic limit, at larger curvature ratios (ε), there is a significant influence of the curvature on the circulation pattern. For instance, in the single-phase problem, this manifests in the bifurcation of the two vortex solution to a four vortex solution as ε (and Re) is increased.[27,28]

The aforementioned discussion provides sufficient motivation to extend the analysis to $O(\varepsilon^2)$. However, the calculation is a detailed one and does not contribute very much to our current goal of undestanding the basic, local features of the flow. Thus we leave the second-order analysis for a future investigation.

Concluding Remarks

Flow of fluids in curved channels has been a topic of interest for several decades. This problem provides an ideal setting for the investigation of centrifugal effects in fluid flow, besides having a variety of applications. The extensive work on the single phase version of this problem has contributed much to the fluid mechanics literature. In this work we present a first theoretical analysis of core-annular two-phase flow in a curved circular channel. We consider a fully developed CA flow with a circular, concentric interface and derive an analytical solution to the problem as a regular asymptotic expansion for the limit of a gently curved channel. This solution is valid for $\varepsilon \ll 1$ and at relatively low Reynolds numbers.

The analysis has revealed several interesting hydrodynamic phenomena which have not been observed in single-phase flows. The interplay of inertial and viscous forces within each fluid is distinct, especially when the properties and volume fractions of the fluids are markedly different. The flow features are enriched by the coupling of the fluids at the fluid–fluid interface. A striking result is the possible reversal of the natural sense of circulation within either fluid. In single-phase flows, the transverse motion, visualized as Dean vortices,[9] has a unique sense of circulation. The flow transports fluid from the inner side to the outer side of the channel along the horizontal centerline of the cross section (Figure 2). In the CA flow, one of the fluids may influence the circulations in the other fluid and reverse the orientation of its vortices. In such a case, fluid will be transported from the outer side of the channel to the inner side along the center of the cross section. This is not conceivable in a single-phase flow. In an intermediate case, the reversal of the transverse flow is localized near the interface which results in the formation of a sandwich vortex between the principle vortices.

The nature of the redistribution of axial velocity is parameter dependent, even in the single phase problem. We provide a physical explanation of the competing *geometric* and *inertial* effects of the axial curvature. The analysis is then extended to the two-phase CA flow. The two curvature effects compete within each fluid and often result in opposing velocity redistribution tendencies. The viscous interfluid coupling at the interface leads to a range of possible velocity redistributions which are dependent on the physical parameters.

The governing physics are understood in greater depth by studying the dependence of the circulation patterns and axial velocity redistribution on the physical parameters. This is done by deriving analytical results for critical transition curves in the parameter space. These are used to organize the 4-D parameter space (Re_1, Re_2, $(\mu_1/\mu_2)$and k) into distinct regions in which different flow regimes occur.

Our consideration of a circular concentric interface imposes a restriction on the capillary number- *Ca* (surface tension parameter). It is not an independent fifth parameter but rather is related to the other four parameters via the condition in Eq. 37. Another way of interpreting the condition of Eq. 37 is that the circular concentric fully developed core solution will be physically observable when the parameters lie on any one of a family of 3-D surfaces parameterized by *Ca*, in the 4-D parameter space. For cases when Eq. 37 is not satisfied, the core will be noncircular and displaced toward the walls of the channel by centrifugal force. However, even in such cases, the insights obtained from this study of the special concentric core case will be useful as guiding principles for future experimental and numerical investigations. For example, one would still observe sandwich vortices and dominated vortices in the flow since the interfluid competition elucidated here will persist even when the core is not concentric. The flow regime maps presented in this work will be useful in the selection of parameter values for targeted experiments and computational fluid dynamics simulations aimed at capturing all the flow features in nonconcentric core-annular flow.

The stability of CA flow in a *curved* channel has *not* yet been addressed theoretically. Stability studies on CA flow in *straight* channels indicate that a CA flow could be stable in a curved channel if the core is relatively large and the flow rates are sufficiently high.[1] Smaller cores can be stable if the core fluid is sufficiently viscous. Stable CA flows have been observed *experimentally* under similar conditions in curved bends.[3,14] Given the potential of curved sections to enhance heat and mass transport in low Reynolds number systems,[7,8] there is considerable motivation to develop a systematic theory of the stability of this flow. Since the theory for straight channels is well developed, the challenge is to understand the effects of the curvature of the channel on the various instability mechanisms- capillary instability, interfacial friction and Reynolds stresses.[29] In addition one must account for the centrifugal instability which has been observed in single-phase curved channel flow.[27] A possible first step could be a linear stability analysis in which the solution presented here is taken as the base flow and subjected to small perturbations.

Literature Cited

1. Joseph DD, Bai R, Chen KP, Renardy YY. Core-annular flows. *Annu Rev Fluid Mech.* 1997;29(1):65–90.
2. Cubaud T, Mason TG. Capillary threads and viscous droplets in square microchannels. *Phys Fluids.* 2008;20(5):053302.
3. Sarkar PS, Singh KK, Shenoy KT, Sinha A, Rao H, Ghosh SK. Liquid-liquid two-phase flow patterns in a serpentine microchannel. *Ind Eng Chem Res.* 2012;51(13):5056–5066.

4. Guillot P, Colin A, Utada A, Ajdari A. Stability of a jet in confined pressure-driven biphasic flows at low Reynolds numbers. *Phys Rev Lett*. 2007;99(104502):1–4.
5. Geschiere SD, Ziemecka I, Van Steijn V, Koper GJM, Esch JH Van Kreutzer MT. Slow growth of the Rayleigh-plateau instability in aqueous two phase systems. *Biomicrofluidics*. 2012;6(2): 22007.
6. Huang Y, Meng T, Guo T, Li W, Yan W, Li X, Wang S, Tong Z. Aqueous two-phase extraction for bovine serum albumin (BSA) with co-laminar flow in a simple coaxial capillary microfluidic device. *Microfluidics Nanofluidics*. 2013. DOI: 10.1007/s10404-013-1245-2.
7. Vashisth S, Kumar V, Nigam KDP. A Review on the potential applications of curved geometries in process industry. *Ind Eng Chem Res*. 2008;47(10):3291–3337.
8. Carlo D Di. Inertial microfluidics. *Lab Chip*. 2009;9(21):3038–46.
9. Dean WR. Note on the motion of fluid in a curved pipe. *Phil Mag*. 1927;7(4):208–223.
10. Dean WR. The stream-line motion of fluid in a curved pipe. *Phil Mag*. 1928;7(5):673–695.
11. Berger SA, Talbot L, Yao LS. Flow in curved pipes. *Annu Rev Fluid Mech*. 1983;15(1):461–512.
12. Muradoglu M, Stone HA. Motion of large bubbles in curved channels. *J Fluid Mech*. 2007;570:455–466.
13. Kumar V, Vashisth S, Hoarau Y, Nigam KDP. Slug flow in curved microreactors: hydrodynamic study. *Chem Eng Sci*. 2007;62(24): 7494–7504.
14. Ghosh S, Das G, Das PK. Simulation of core annular in return bends-A comprehensive CFD study. *Chem Eng Res Des*. 2011;89: 2244–2253.
15. Ellenberger J, Hart J, Hamersma PJ. Single- and two- phase flow through helically coiled tubes. *Chem Eng Sci*. 1988;43(4):775–783.
16. Bandaru SVSRK, Rajendra P. Pressure drop for single and two-phase flow of non-newtonian liquids in helical coils. *Can J Chem Eng*. 2002;80:315–321.
17. Kirpalani DM, Patel T, Mehrani P, Macchi A. Experimental analysis of the unit cell approach for two-phase flow dynamics in curved flow channels. *Int J Heat Mass Tran*. 2008;51(5-6):1095–1103.
18. Donaldson AA, Kirpalani DM, Macchi A. Curvature induced flow pattern transitions in serpentine mini-channels. *Int J Multiphas Flow*. 2011;37(5):429–439.
19. Wang C-C, Chen IY, Yang Y-W, Chang Y-J. Two-phase flow pattern in small diameter tubes with the presence of horizontal return bend. *Int J Heat Mass Tran*. 2003;46(16):2975–2981.
20. Topakoglu HC. Steady laminar flow of an incompressible viscous fluid in curved pipes. *J Math Mech*. 1967;16(12):1321–1337.
21. Leal LG. Advanced Transport Phenomena-Fluid Mechanics and Convective Transport Processes. New York: Cambridge University Press; 2007.
22. Dean WR. Fluid motion in a curved channel. *P Roy Soc A-Math Phy*. 1928;121(787):402–420.
23. Reid WH. On the stability of viscous flow in a curved channel. *P Roy Soc A-Math Phy*. 1958;244(1237):186–198.
24. Sparrow EM. On the onset of flow instability in a curved channel of arbitrary height. *ZAMP*. 1964;15:638–642.
25. Cuming HG. The Secondary Flow in Curved Pipes. London, UK: Aeronautical Research Council, Her Majesty's Stationery Office; 1952.
26. De Vriend HJ. Velocity redistribution in curved rectangular channels. *J Fluid Mech*. 1981;107:423–439.
27. Nandakumar K, Masliyah JH. Bifurcation in steady laminar flow through curved tubes. *J Fluid Mech*. 1982;119:475–490.
28. Winters KH. A bifurcation study of laminar flow in a curved tube of rectangular cross-section. *J Fluid Mech*. 1987;180:343–369.
29. Howard HH, Joseph DD. Lubricated pipelining: stability of core-annular flow. *Part 2. J. Fluid Mech*. 1989;205:359–396.

Manuscript received Mar. 4, 2013; and revision received Sept. 9, 2013.